The Design of a System for the Induction Hardening of Steels Using Simulation Parameters

Zoran Stević [1,2], Stevan P. Dimitrijević [3], Miša Stević [4], Predrag Stolić [1], Sanja J. Petrović [5,*], Milan Radivojević [5] and Ilija Radovanović [2,6]

1   Technical Faculty in Bor, University of Belgrade, Vojske Jugoslavije 12, 19210 Bor, Serbia;
    zstevic@tfbor.bg.ac.rs (Z.S.); pstolic@tfbor.bg.ac.rs (P.S.)
2   School of Electrical Engineering, University of Belgrade, Bulevar Kralja Aleksandra 73, 11120 Belgrade, Serbia;
    ilija.radovanovic@ic.etf.bg.ac.rs
3   Innovation Centre of Faculty of Technology and Metallurgy, University of Belgrade, Karnegijeva 4,
    11120 Belgrade, Serbia; sdimitrijevic@tmf.bg.ac.rs
4   Elsys Eastern Europe, Omladinskih Brigada 90e, 11070 Belgrade, Serbia; stevic.ext@ic.etf.bg.ac.rs
5   Mining and Metallurgy Institute Bor, Zeleni Bulevar 35, 19210 Bor, Serbia; milan.radivojevic@irmbor.co.rs
6   Innovation Centre of the School of Electrical Engineering in Belgrade, Bulevar Kralja Aleksandra 73,
    11120 Belgrade, Serbia
*   Correspondence: sanja.bugarinovic@irmbor.co.rs

Abstract: This paper presents the development of a piece of induction hardening equipment based on the foundations of the design, starting from zero. It was intended for steels in general, and was tested on unalloyed low- and medium-carbon steels, whereas the results for EN 1C60 steel are shown in this study. The EN 1C60 steel showed average results, and was chosen as a representative of a wider group of engineering steels. The main objective of this work was to develop a flexible system for mild steel hardening that can be used for various hardening depths and steel types. The system design's priorities were the use of standard electronic components to avoid supply chain disruptions and to achieve high energy efficiency. The construction of the prototype in full detail is also presented. The optimal process parameters are listed, as well as the procedure of their obtaining by using the appropriate simulation method. The key parameters were adjusted in consecutive steps. This study resulted in high matching between the model predictions and experimental results. The basic goal of this research was achieved, with the system having a minimum energy efficiency of 75.3%, a most frequent energy efficiency of 90% and a maximum energy efficiency of 95.1%.

Keywords: induction hardening; energy efficiency; design; simulation; half-bridge inverter

1. Introduction

Induction furnaces have been used since the first decade of the 20th century (USA and Germany), and a new generation of these furnaces was developed in the mid-1980s [1]. There are two main types of induction furnaces: coreless and channel [2].

A coreless induction furnace contains a coil made of copper tubing, wound into a spiral shape [3]. This type of furnace can be used for a wide range of metals and alloys, and it is the most widely used today. In order to cool the coil, water circulates through it, which is then cooled in the cooling system (forced air circulation) [4,5].

Today, induction furnaces that operate at medium frequencies (a few hundred Hz to a few tens of kHz) are mostly in use, and inverters are used for their power supply [6–11].

The concept of the electromagnetic processing of materials originates from the 1980s [12]. It includes the following areas of application in material processing: annealing, precipitation hardening, surface hardening, normalizing, soldering and hardening [13–16].

The induction heating of the internal surfaces of workpieces can be used for a variety of applications such as hardening, tempering, annealing, shrinking, stress reduction and

brazing. Certain different types of inductors for heating the internal surfaces of processed workpieces are shown in Figure 1 [17].
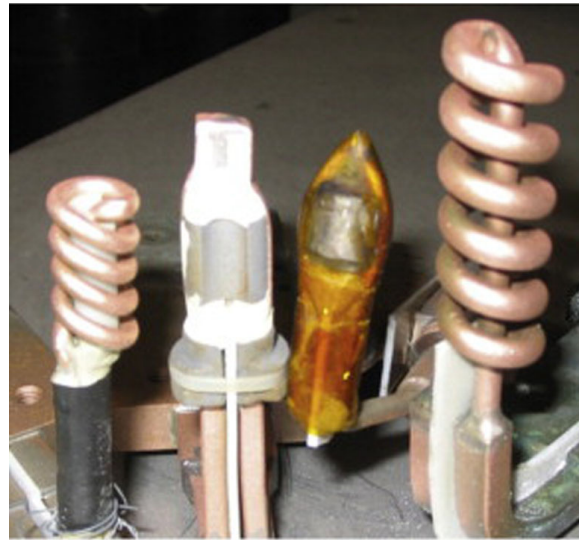

Figure 1. Inductors for hardening the inside of workpieces [Reproduced with permission from [17]; published by Elsevier, (2014)].

Converters containing a rectifier circuit for rectifying the mains supply and an inverter for obtaining an alternating current of increased frequency are used to supply the inductor. Depending on the method of providing the load, inverters can be voltage source inverters (VSIs) or current source inverters (CSIs). The output voltage of the voltage inverter consists of a train of voltage pulses that are shaped by the pulse duration modulation process. Using a simple periodic modulating signal, the spectrum of the inverter output voltage consists of the fundamental harmonic, which is the desired voltage on the load, and a series of unwanted higher harmonics removed by a low-frequency bandpass filter [18].

The converter with a half-bridge voltage inverter system, usually used for powers of the order of tens of kW, is presented in Figure 2.
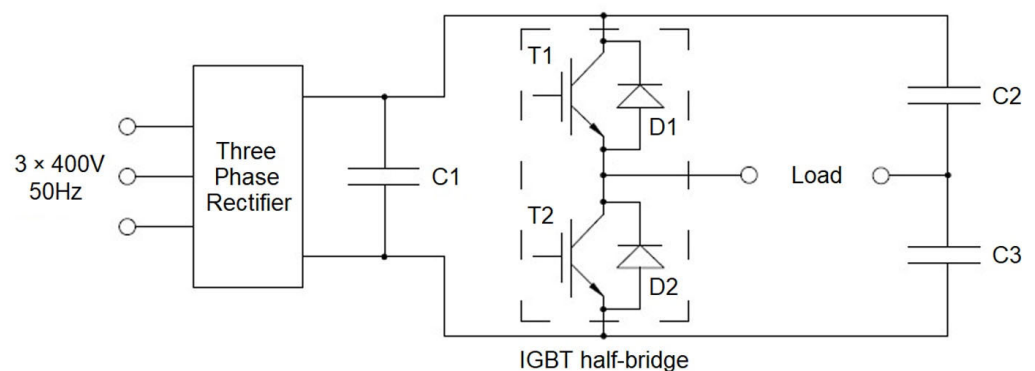

Figure 2. Principle scheme of the converter.

The converter consists of a three-phase diode rectifier, filter capacitor C1, transistor half-bridge and resonant capacitors C2 and C3. An inductor is connected between the open contacts in the diagram.

Among the numerous ferromagnetic and non-ferromagnetic materials that are thermally processed, steel is of particular importance because of its mechanical qualities—strength and toughness. In some industrial applications, however, its properties are not entirely satisfactory, so it must be modified inhomogeneously. For example, the steel shafts of large electric motors require a high outer layer hardness and the sufficient preservation

of core toughness. This can be achieved through the process of surface hardening, which should be applied so that the interior of the shaft maintains good elasticity [19].

Hardening is a heat treatment process that involves the following steps:

- Heating the steel to a temperature slightly above the critical temperature;
- Holding the steel at this temperature until complete normalization and the completion of structural transformations;
- Cooling the steel at a rate necessary to obtain the martensitic structure that gives the steel excellent hardness.

Hardened steel is characterized by high hardness, great brittleness and significant internal stress. The steel parts must be loosened after hardening to reduce these stresses.

Induction hardening is the most commonly used surface hardening method due to its high productivity and the high quality of the hardened layer. Heating with a high-frequency current is based on the so-called "skin effect" phenomenon. The surface layers of the steel part heat up rapidly to high temperatures, while the inner layers remain cold or heat up only slightly due to the thermal conductivity of the steel. An alternative high-quality method is laser surface hardening, but this involves higher costs and has limited applications compared to the induction method [20]. Another relatively modern method is electron beam hardening. Similar to the previous method, the interaction of the beam and material generates heat in the surface layer of the sample. Although it has advantages over the laser method, its comparatively low energy efficiency (even over 70%) [21], high investment costs and the creation of significant artefacts in X-ray computed tomography images (in the control or process of the material analysis) [22] are substantial disadvantages compared to the induction process.

The maximum hardness achieved during induction hardening is 2–3 HRC units higher than during classical heating in a furnace. Other mechanical properties of steel (tensile strength, yield strength, elongation, contraction and impact toughness) also show higher values after induction hardening than after classical hardening [19].

The additional advantages of induction hardening compared to classic hardening are as follows:

- Lower energy consumption;
- Higher productivity;
- The greater possibility of automating the process;
- Higher-quality tempered steel;
- Less material deformation.

Some of the most important elements of industrial plants where the induction hardening of steel is applied include electric motor shafts, gears, crankshafts, turbine blades, rolling mill rolls, gauges and tools operating under impact loads.

Although induction hardening is a mature technology, it constantly evolves and finds new contemporary applications. A good example is its use in hybrid or duplex technologies, where mechanical and surface thermal processes or two different heat treatment processes are combined, which can considerably increase the processing capacity, as shown in a recently published article [23]. Other implementations include additive manufacturing [24], supporting sustainability in the manufacturing of some mechanical components [25] and further optimization of the high-frequency process, considering the metal phase transformation simulations [26].

Finally, it should be emphasized that induction hardening belongs to the complex multiphysics parameterized problems [27], and thus, it is highly complicated for calculation and simulation. Different approaches have been used to simulate the process: using an algorithm scheme [28], the finite element method [29], various numerical modelling with multiparameter material properties [30], data-driven analysis with applied multi-linear regression [31], or the nonlinear regression technique [27] and neural networks [32].

In terms of energy efficiency, a high-power resonant full-bridge inverter (FBRI) can easily reach a maximal efficiency of 95% at high frequencies [33], but when applied for

induction hardening, a similar FBRI at full load in the kW range could achieve a much lower efficiency of 85% [34]. A higher efficiency for induction hardening could be achieved using a particular test setup, with an approach relying on efficiency maximization, leading to an efficiency of up to 91% [35]. An efficiency above 95% is reserved for low-temperature applications, where even 97% efficiency is achievable [36]. However, in induction hardening, only special systems like dual-frequency induction heating (efficiency of the inverter up to 96%) [37] can reach the goal. Therefore, any result above 90% should be considered high efficiency for the application.

The presented study aims to develop a new system for induction hardening, using the design from scratch, with an energy efficiency of over 90% as the primary goal. System optimization has improved this development through the correction of parameters by comparing simulation and experimental results. The use of a general electronic simulation program to optimize parameters without a complex mathematical model or without the need for machine learning is considered to be the main novelty of the presented work. By following this approach, the optimization of the actual system is achieved based on the simulation results, which, in addition to high energy efficiency, is a significant contribution to the development of such systems.

2. Materials and Methods

This research included the development to the prototype level of an induction hardening system, and its testing, optimization based on modeling and simulation, the maximization of the degree of utilization, as well as practical application in real conditions.

2.1. Realization of the Prototype System for Induction Hardening

A circuit diagram of the system for the induction hardening of steel with the following characteristics is shown in Figure 3:

- Power supply: 3×400 V, 50 Hz;
- Nominal power: 15 kW;
- The inductance of the inductor coil: 32–50 μH;
- Maximum energy efficiency: 95%;
- Output frequency: 10–25 kHz.

The output frequency has varied in the range of 10–25 kHz to adjust the resonant frequency for different inductors and penetration depths.

The three-phase mains voltage is supplied to the diode rectifier via the soft start circuit. From the rectifier, through the DC link (bus with voltage filtering capacitors), DC power is supplied to the input of the inverter.

The inverter, depending on the parameters of the resonant circuit and the set operating frequency, with the help of the control circuit and switching elements, provides an alternating high-frequency voltage at its output. An inductor is connected to the output of the inverter, inside which there is a cylindrical steel batch, which is the subject of heat treatment (hardening). The LEM current sensor monitors the inductor current, displays it on the display and defines the overload limit.

Due to the highly pronounced skin effect, the inductor is made of a hollow copper conductor. The losses in copper are relatively high due to the small effective cross-section through which the current flows. The inductor is cooled with water flow, and the water is cooled with airflow using a fan. Additionally, there is a fan that cools the converter components. The entire power supply system is placed in an electrical cabinet together with automatic fuses, switches, a soft start device, cooling units and signaling (Figure 4).
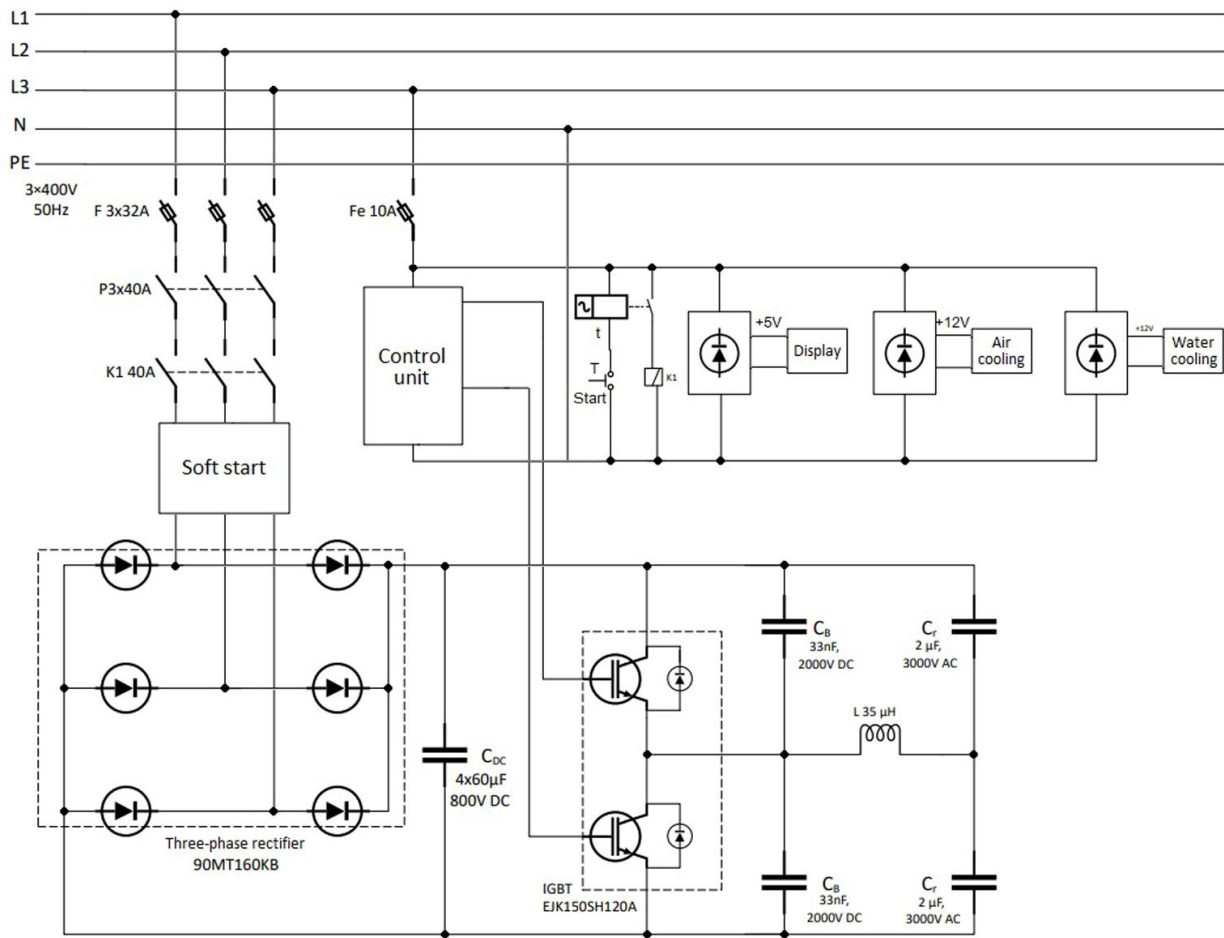
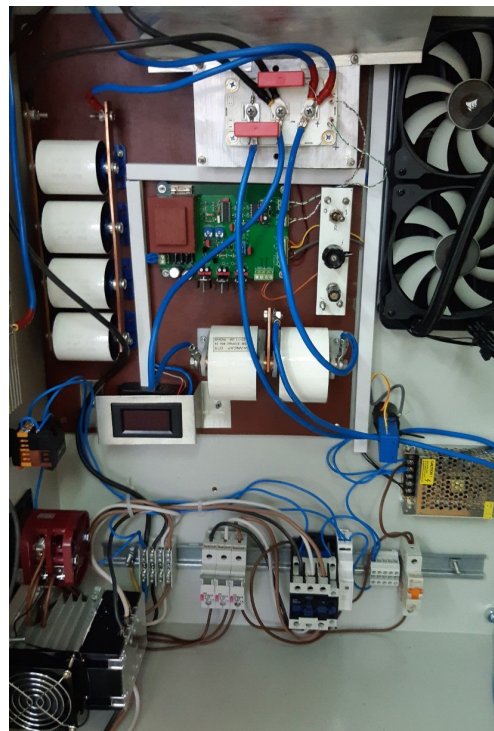**Figure 3.** Electrical diagram of the induction hardening system.

Figure 4. The layout of the electrical cabinet.

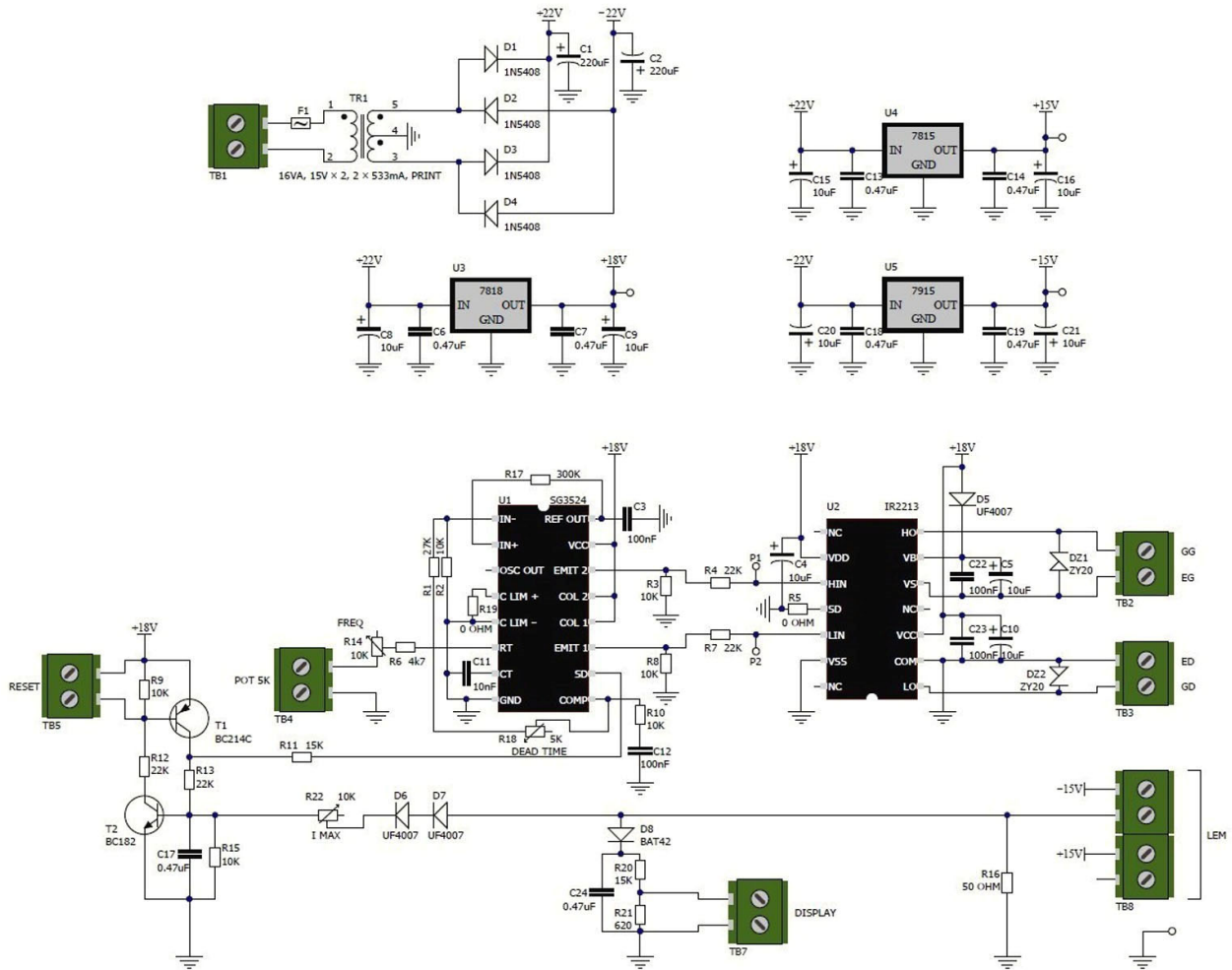The original design of the control unit is presented in Figures 5 and 6.

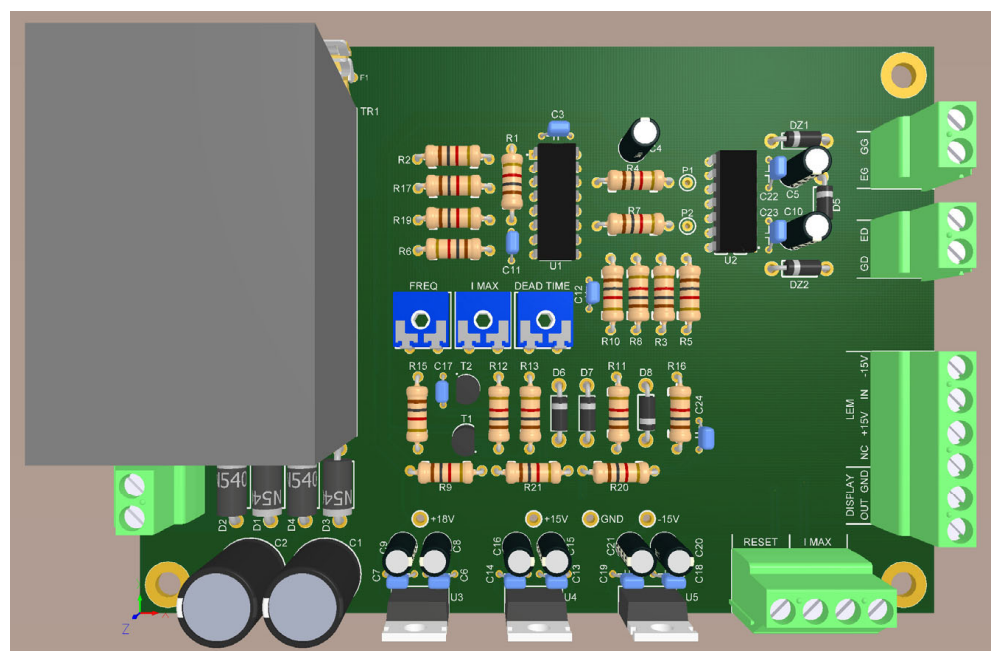**Figure 5.** Electrical scheme of the control part.

Figure 6. Three-dimensional model of the control module.

The classic rectifier circuit (transformer TR1, diodes D1 to D4 and filter electrolytic capacitors C1 and C2) provides DC voltages of ±22V for supplying stabilized power supplies of +18V based on IC 7818, as well as ±15V based on IC 7815 and 7915, with additional filtration (capacitors C6 to C21).

The PWM control signal generator is based on IC SG3524 (U1) [38] with accompanying passive components. The SG3524 is a pulse width modulation (PWM) set frequency control circuit. The frequency is adjusted by an external RC branch, formed of R6, R14 and C11. The circuit also contains a current-limiting comparator and output pulse suppression circuitry. The output signals from SG3524 are fed to the IGBT driver input pins "HIN" and "LIN" of the IR2213 IC (U2) for the upper (high) and lower (low) IGBT control.

The IGBT drivers are integrated into IC IR2213 [39]. The IR2213 is a high-voltage, high-speed driver designed for IGBT and MOSFET transistors used in power electronics. It contains two independently referenced output channels (high-side and low-side). It is suitable for applications at high frequencies and voltages up to 1200 V.

The circuit also contains a current-limiting comparator and output pulse suppression circuitry, consisting of transistors T1 and T2 and accompanying passive components. The output conductor to the inductor is covered by a Hall effect-based current sensor (LEM), which provides a voltage output proportional to the output current. The signal from the current sensor is wired via a terminal block connector labeled as TB8, thus providing the control signal for the transistor circuit and the output current display (DISPLAY). In the case of overcurrent or the need for a manual reset, the transistor circuit stops the pulse generation by providing the signal to the SD (shutdown) pin of SG3524. The output current display is always active and shows the output current value in real time.

2.2. Inductor and Batch Modeling

For a suitable calculation, the required information is the dimensions and materials of the inductor and the batch, the number of turns of the inductor, the frequency of the supply and the operating temperature. The data are as follows:

- Batch: carbon steel;
- Inductor diameter: D_{ind} = 100 mm;
- Inductor length: h_{ind} = 800 mm;
- Number of inductor turns: 60;
- Batch diameter: D_{ch} = 35 mm;
- Power supply frequency: 10–25 kHz;
- Maximum batch temperature: 800 °C.

A transformer model was adopted, where the inductor represents the primary, with N turns, and the batch is the secondary, with one short-circuited turn. Therefore, the inductor and the load can be represented by a series branch, equivalent resistance and inductance [40,41].

The inductance of an inductor can be measured with an L-meter, with several items to consider. Since the charge is ferromagnetic, a higher inductance is expected when it is placed inside the inductor. Also, with an increase in temperature (up to Curie for steel), depending on the power supply frequency, the inductance can take values higher than those measured. Therefore, the measured value of the inductance will be taken as the initial one for the simulation, and corrections will be made exclusively in the direction of increasing that value, by using an iterative method, until a result of satisfactory accuracy is reached. The initial (measured) value of the equivalent series inductance was 32 μH.

For the calculation of the equivalent resistance of the inductor and the batch, it is necessary to know the specific resistance of the materials at the appropriate temperatures and the depth of current penetration at the proper operating frequency for the given materials.

In simple terms, the inductor will be considered to be at a temperature of 80 °C (because it is separated from the batch with ceramics and cooled with water), while the batch temperature is 800 °C. The specific electrical resistance of copper (ρ_{ind}) at the working

temperature of the coil is $2.07 \cdot 10^{-8}$ Ωm. The specific resistance of carbon steel (ρ_{ch}), at 800 °C, at the indicated power supply frequency is $115.1 \cdot 10^{-8}$ Ωm.

The equivalent series resistance of the inductor and the ferromagnetic charge is calculated according to the following equation [23]:

$$R_{ind,ch} \approx 1.3 \cdot \pi \cdot \rho_{ind} \cdot N_{ind}^2 \cdot \frac{F_{ind}}{z_{ind} \cdot h_{ind}} + \rho_{ch} \cdot N_{ind}^2 \cdot \frac{F_{ch} \cdot \pi}{z_{ch} \cdot h_{ind}} \tag{1}$$

where N_{ind} represents the number of turns of the inductor, while z_{ind} and z_{ch} represent the depths of Foucault's currents in the conductor of the inductor and in the batch, respectively. The first addend represents the equivalent series resistance of the inductor at 80 °C, and the second addend represents the equivalent resistance of the steel batch (reduced to the inductor side) at 800 °C.

Based on the tables and calculations [41], $z_{ind} \approx 1$ mm and $z_{ch} \approx 3.3$ mm were obtained. This determined the serial resistance value of the LR branch $R_{ind,ch}$ = 205.4 mΩ. That resistance value was taken (as in the case of inductance) as the initial value for the simulation. Then, it was increased using an iterative method until satisfactory accuracy was achieved.

2.3. Energy Efficiency

The degree of utilization of the induction heating power is defined as the ratio of the power that raises the temperature of the batch, according to the total electrical power supplied to the converter:

$$\eta = \frac{P_{heat}}{P_{net}} \tag{2}$$

where P_{heat} is calculated as

$$P_{heat} = R_{ind,ch} \times I_{ind\ eff}^2 \tag{3}$$

where $I_{ind\ eff}$ is the effective current through the inductor.

In the optimal case (described inductor completely filled with steel charge, good thermal insulation, heating below the Curie temperature, frequency slightly lower than the resonant frequency, inverter in the optimal range, etc.), the following parameters were measured and calculated:

- Network power consumption: P_{net} = 12.87 kW;
- DC link voltage: V_{DC} = 250 V;
- DC link current: I_{DC} = 50.92 A;
- Inductor effective current: $I_{ind\ eff}$ = 120 A;
- Equivalent serial resistance: $R_{ind,ch}$ = 0.85 Ω;
- Power of induction heating: $P_{heat} = 0.85 \times 120^2$ = 12.24 kW.

According to the previous measurements and calculations, the energy efficiency can be calculated:

$$\eta = \frac{12.24}{12.87} = 0.951 = 95.1\% \tag{4}$$

2.4. Simulation of a Half-Bridge Resonant Inverter

The simulation of the system for the induction hardening of steel with a single-phase half-bridge voltage inverter was carried out in the TINA program from Texas Instruments (Version: 9.3.200.277), which is based on the SPICE (Simulation Program with Integrated Circuit Emphasis) and serves for the simulation of analogue and digital electrical circuits, as well as for the design of printed circuit boards. It enables the efficient performance of all conventional types of electronic circuit analysis.

The frequency in the control circuit has a wide adjustment range, but in this work, frequencies in the range of f = 10 to 25 kHz were used, which was the resonant frequency of the shown inverter. The inductance L (pure inductive load) value was set to 32 μH, which

was determined through direct measurement; however, it varies up to 50 µH due to batch and other factors.

2.5. Simulation Scheme and Parameters

In order to simplify the simulation, the rectifier bridge and the DC link in the scheme are replaced by an ideal voltage source. The value of the source voltage (V1) depends on the effective value of the voltage in the DC intermediate circuit. Capacitors in parallel with switches are eliminated in this case, considering that, in the simplified version, ideal switches are used instead of IGBT transistors (all parasitic effects are neglected). The rise, fall and dead time are ignored in the control signal. A simplified scheme is shown in Figure 7, and further results and conclusions are drawn based on the previous.
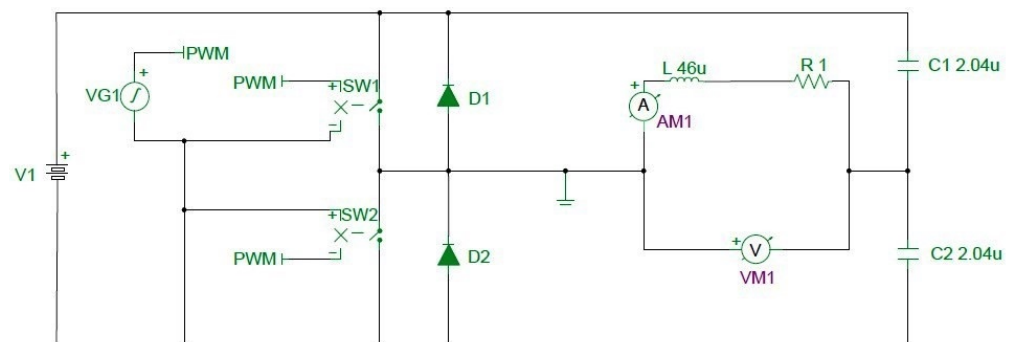

Figure 7. Simplified diagram of a half-bridge resonant inverter.

After determining the basic parameters of the equivalent electric circuit, as well as the voltage on the DC link, which was 250 V in the experiment, the simulation was started.

In order to observe the voltage and current waveforms of the inductor, a transient analysis was required, while an AC analysis was required to determine the resonant frequency. The resonant frequency fr = 11.68 kHz was determined for the initial values of the circuit parameters.

3. Results and Discussion

It was concluded that the initial parameters were satisfactory for a relatively faithful representation of the waveforms from the experiment, using the iterative method of changing the value of the resistance and inductance of the series branch in the simulation model. A further increase in the resistive load would reduce the voltage on the inductor. A further increase in the inductive load would change the resonant frequency of the oscillator circuit vitally, and the waveforms would change their appearance more drastically.

The experiments were performed at different voltage values on the DC link and the same inductor, as described previously, but the optimization was performed at $V_{DC} = 250$ V. Firstly, the experimental results will be presented, followed by the simulation results for the same experimental conditions.

The additional measuring equipment is shown in Table 1.

Table 1. The additional measuring equipment.

Measurement	Equipment
V, I, R, L	0.1% class instruments
Waveform, frequency	Oscilloscope ROHDE & SCHWARZ RTB2004 (Munich, Germany)
Power (active, reactive)	Digital Energy meter Saving Electronics DTSU 1218 (Jiangsu, China)
Temperature	Thermography camera FLIR T420, FLIR Systems, Inc., (Santa Barbara, CA, USA)

A corresponding graph of the voltage and current waveforms of the inductor at a DC link voltage of 250 V, with the values of the relevant parameters, is shown in Figure 8.

The yellow line indicates the voltage and the green line indicates the current. The circuit operated at a frequency of 11.22 kHz.

Figure 8. Measured voltage and current waveforms from the experiment.

In Figure 8, perceptibly, the amplitude of the voltage on the inductor was about 610 V, while the amplitude of the current was about 155 A. Under the mentioned conditions in the experiment, the current from the network was 36 A, and the measured active power was P = 3360 W.

Figure 8 also shows that the circuit in the experiment was operating at a frequency lower than the resonant frequency. Due to the fact that the DC link voltage is constant, setting the operating frequency closer or further from the resonant frequency is an efficient way to control the output power.

The results of the transient analysis of the simulated circuit under the same conditions as in the experiment are shown in Figure 9.
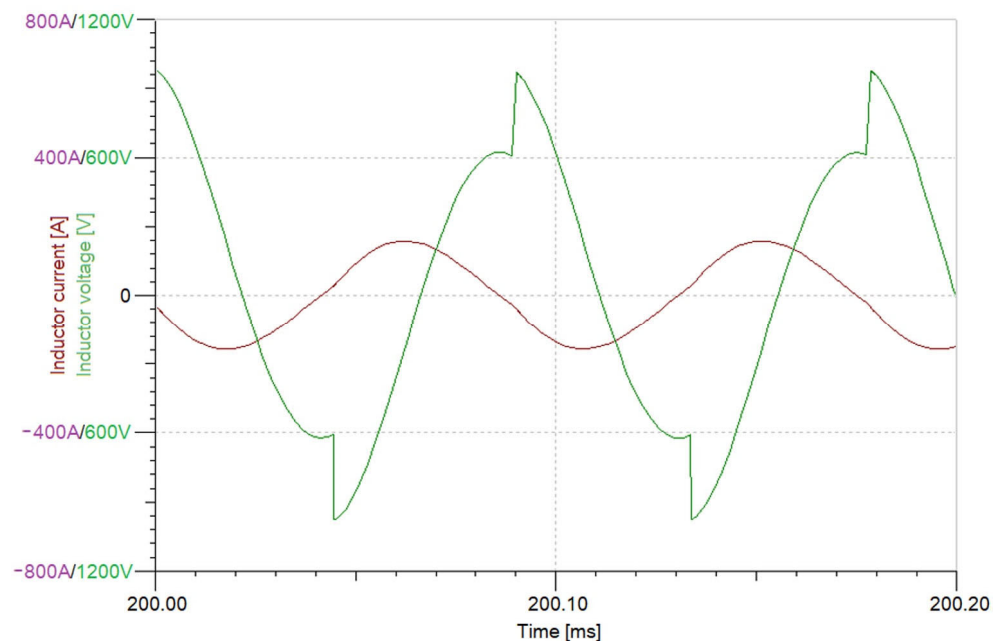

Figure 9. Simulated waveforms of the voltage and current of the inductor at the voltage of the DC intermediate circuit (250 V) and the pulse width modulation frequency (11.22 kHz < frez = 11.68 kHz).

In addition to the qualitative comparison (signal shape, for example), a quantitative comparison of the characteristic values was performed, and they are shown in Table 2.

Table 2. Quantitative comparison of the characteristic values obtained through measurements and simulations.

Parameter	Measurement	Simulation
Maximum inductor current [A]	154.7	158.5
Maximum inductor voltage [V]	610.4	618.2
Voltage spike [V]	415.3	396.2

Assuming that the actual resistance of the batch is equal to the calculated one, the efficiency coefficient of the system would be about 76.6%. Parasitic effects significantly influence that factor, so the actual value lies in the interval between 75.3% and 95.1%. Maximum efficiency is achieved in optimal conditions, as described in 2.3.

The parameters obtained in this research in comparison with related research results are shown in Table 3 [35,37].

Table 3. The results of this research in comparison with related research.

Parameter	This Research	Reference [35]	Reference [37]
Nominal power (kW)	15	10	0.05
Output frequency (kHz)	10–25	10–50	50
Max. utilization rate (%)	95.1	91	97

A series of images were taken with a thermal imaging camera in order to form the heating curves of the batch. One of the images from the thermal imaging camera is shown in Figure 10, showing that the steel reached a temperature of 680 °C. The temperature ranged from 211.4 °C to 904.2 °C (Figure 11).
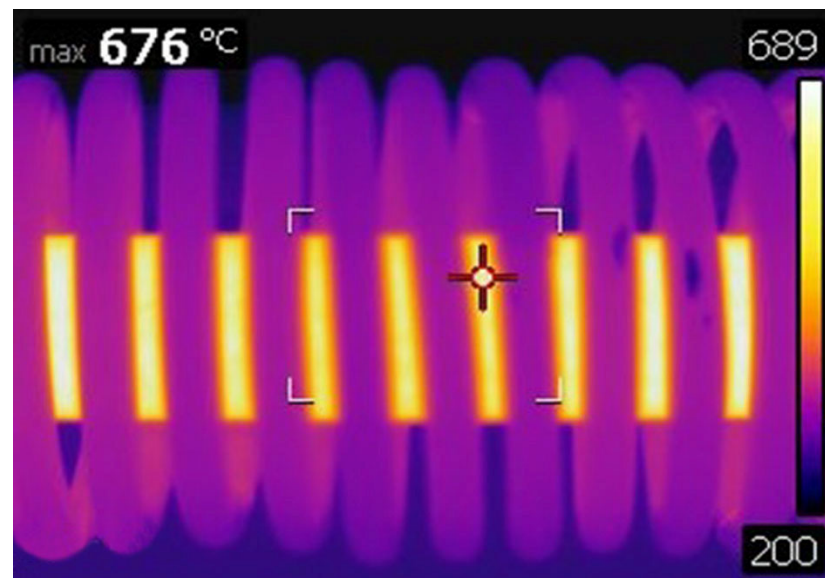

Figure 10. A recording of the experiment with a thermal imaging camera.

Based on the graph, it can be estimated that the temperature would enter a stationary state under the mentioned conditions. After a few minutes, it would remain at a value of about 1000 °C. A photo of the red-hot steel in the process of hardening is given in Figure 12.
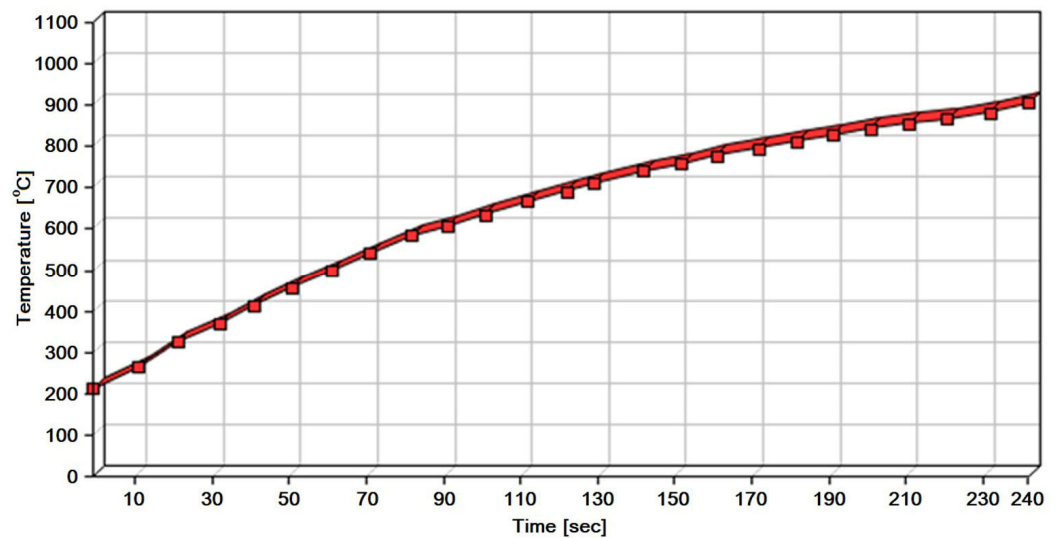
Figure 11. Graph of the time dependence of the temperature of the steel batch based on a series of images from a thermal imaging camera during the experiment at a DC intermediate circuit voltage of 250 V.

Figure 12. Photograph of a red-hot object of hardening.

The system was also tested in a real industrial environment, where it was used to heat large machine parts in heavy-duty machinery assembly processes. For that purpose, the mounting part had to be heated uniformly at 250 °C. Instead of a copper tube, a multi-strand enameled copper wire was used to form an inductor due to practicality reasons. As the system operates at a relatively low frequency, thus achieving a larger penetration depth, the conducted industrial environment tests proved that the system is ideal for this purpose. A photo of the copper wire coil, wound up around the machine part, is shown in Figure 13.

Figure 13. Application in industrial environment.

4. Conclusions

A prototype system for induction hardening with a power of 15 kW and a frequency of 10 to 25 kHz was designed and implemented. The main results of the study are as follows:

- The use of simulation was successfully performed for the system optimization. The parameters from the simulation had differences ranging from 1.3% to 4.8% compared to the measurements in the application of the equipment;
- The optimized system achieves impressive utilization rates between 75.3% and 95.1%;
- The designed system achieved the goals of flexibility since it was used for various steel grades, and was inexpensive and economical in use as well as being portable.

The energy efficiency results represent a significant advance in the efficiency of the induction hardening process, which positively impacts various industries that use such methods to improve the mechanical characteristics of their products. It also presents a good base for lowering carbon footprints and bringing us closer to the circular economy goals of the induction hardening processes.

By introducing this system into industrial processes, it is expected to increase production efficiency, reduce costs and improve the quality of hardened products. The system is suitable for additional adjustments using machine learning methods by collecting and analyzing data from actual applications. Further research and development can lead to even better results and broader applications of induction hardening in various industries.

Institutional Review Board Statement: Not applicable.

Informed Consent Statement: Not applicable.

References

1. Gandhewar, V.R.; Bansod, S.V.; Borade, A.B. Induction Furnace: A Review. *Int. J. Eng. Technol.* **2011**, *3*, 277–284.
2. Mühlbauer, A. *History of Induction Heating and Melting*; Vulkan-Verlag GmbH: Essen, Germany, 2008.
3. Schmitz, W.; Trauzeddel, D. Latest Developments in Recycling Production Residues Employing Coreless Induction Furnaces. In Proceedings of the European Metallurgical Conference - EMC 2013, Weimar, Germany, 23–26 June 2013.
4. ECM-FURNACES. Available online: https://www.ecm-furnaces.com/induction-melting-furnaces/laboratory-induction-furnace (accessed on 1 July 2023).
5. Brogden, S.D. Applications for Induction Furnaces in Manufacturing Technology Courses. Ph.D. Thesis, California State University, Fresno, CA, USA, 2015.
6. Hang, N.T.T.; Lüdtke, U. Numerical Simulation of Induction Channel Furnace to Investigate Efficiency for low Frequencies. *Proc. IOP Conf. Ser. Mater. Sci. Eng.* **2018**, *355*, 012012. [CrossRef]
7. Hou, Y.J.; Tian, H.M.; Qu, X.D.; Teng, J.Z.; Liu, G.X.; Li, Y. Development of digital control system for medium frequency induction furnaces. *Proc. IOP Conf. Ser. Earth Environ. Sci.* **2018**, *188*, 012005. [CrossRef]
8. Solanki, V.; Joshi, S.R.; Chavda, J.; Mokariya, K. Simulation of Induction Furnace and Comparison with Actual Induction Furnace. *Int. J. Recent Technol. Eng.* **2013**, *2*, 105–109.
9. Gbadamosi, S.L.; Melodi, A.O. Harmonic distortion from induction furnace loads in a steel production plant. *Netw. Complex Syst.* **2013**, *3*, 8–16.
10. Yılmaz, İ.; Durna, E.; Ermiş, M. Design and Implementation of a Hybrid System for the Mitigation of PQ Problems of Medium-Frequency Induction Steel-Melting Furnaces. *IEEE Trans. Ind. Appl.* **2016**, *52*, 2700–2713. [CrossRef]
11. Tan, A. Modeling and Analysis of Power Quality Compensation Systems for Current Source Inverter Based Induction Furnace. Master's Thesis, Institute of Natural and Applied Sciences, Çukurova University, Adana, Turkey, 2011.
12. Asai, S. Birth and Recent Activities of Electromagnetic Processing of Materials. *ISIJ Int.* **1989**, *29*, 981–992. [CrossRef]
13. Biesuz, M.; Saunders, T.; Ke, D.; Reece, M.J.; Hu, C.; Grasso, S. A review of electromagnetic processing of materials (EPM): Heating, sintering, joining and forming. *J. Mater. Sci. Technol.* **2021**, *69*, 239–272. [CrossRef]
14. Moghanizadeh, A.; Ashrafizadeh, F.; Bazmara, M. Development the Flexible Magnetic Abrasive Finishing Process by Transmitting the Magnetic Fields. *Int. J. Adv. Manuf. Technol.* **2022**, *119*, 2115–2125. [CrossRef]
15. Marczak, M.; Zawora, J. Finite Element Analysis of the Magnetic Field Distribution in a Magnetic Abrasive Finishing Station and its Impact on the Effects of Finishing Stainless Steel AISI 304L. *Metals* **2021**, *11*, 194. [CrossRef]
16. Michalowska, J.; Józwik, J. Prediction of the Parameters of Magnetic Field of CNC Machine Tools. *Prz. Elektrotech.* **2019**, *95*, 134–136. [CrossRef]
17. Rudnev, V.I.; Loveless, D. 12.15—Induction Hardening: Technology, Process Design, and Computer Modeling. In *Comprehensive Materials Processing*; Hashmi, S., Batalha, G.F., Van Tyne, C.J., Yilbas, B., Eds.; Elsevier: Amsterdam, The Netherlands, 2014; Volume 12, pp. 489–580.
18. Wu, B. *High-Power Converters and AC Drives*; John Wiley & Sons, Inc.: Hoboken, NJ, USA, 2006.
19. Remya, M.N.; Barai, M. Study of Induction Heating using Half Bridge Series Resonant Inverter. *Int. J. Sci. Eng. Res.* **2018**, *9*, 1520–1526.
20. Babu, P.D.; Balasubramanian, K.R.; Buvanashekaran, G. Laser Surface Hardening: A review. *Int. J. Surf. Sci. Eng.* **2011**, *5*, 131–151. [CrossRef]
21. Choo, S.-H.; Lee, S.; Golkovski, M.G. Effects of Accelerated Electron Beam Irradiation on Surface Hardening and Fatigue Properties in an AISI 4140 Steel used for Automotive Crankshaft. *Mater. Sci. Eng.* **2000**, *293*, 56–70. [CrossRef]
22. Ahmed, O.M.H.; Song, Y. A Review of Common Beam Hardening Correction Methods for Industrial X-ray Computed Tomography. *Sains Malays.* **2018**, *47*, 1883–1890. [CrossRef]
23. Skeeba, V.Y.; Ivancivsky, V.V.; Martyushev, N.V. Peculiarities of High-Energy Induction Heating during Surface Hardening in Hybrid Processing Conditions. *Metals* **2021**, *11*, 1354. [CrossRef]
24. Eastwood, M.D.; Haapala, K.R. An Induction Hardening Process Model to Assist Sustainability Assessment of a Steel Bevel Gear. *Int. J. Adv. Manuf. Technol.* **2015**, *80*, 1113–1125. [CrossRef]
25. Brøtan, V.; Berg, O.Å.; Sørby, K. Additive Manufacturing for Enhanced Performance of Molds. *Procedia CIRP* **2016**, *54*, 186–190. [CrossRef]
26. Choi, J.; Lee, S. High-Frequency Heat Treatment of AISI 1045 Specimens and Current Calculations of the Induction Heating Coil Using Metal Phase Transformation Simulations. *Metals* **2020**, *10*, 1484. [CrossRef]

27. Derouiche, K.; Garois, S.; Champaney, V.; Daoud, M.; Traidi, K.; Chinesta, F. Data-Driven Modeling for Multiphysics Parametrized Problems-Application to Induction Hardening Process. *Metals* **2021**, *11*, 738. [CrossRef]

28. Cajner, F.; Smoljan, B.; Landek, D. Computer simulation of induction hardening. *J. Mater. Process. Technol.* **2004**, *157–158*, 55–60. [CrossRef]

29. Zhou, H.; Zhao, D.; Liu, Y.; Li, G. Influence of Induction Hardening Process on Camshafts' Residual Stresses. *Arab. J. Sci. Eng.* **2020**, *45*, 9651–9659. [CrossRef]

30. Tong, D.; Gu, J.; Yang, F. Numerical simulation on induction heat treatment process of a shaft part: Involving induction hardening and tempering. *J. Mater. Process. Technol.* **2018**, *262*, 277–289. [CrossRef]

31. Garois, S.; Daoud, M.; Chinesta, F. Data-Driven Inverse Problem for Optimizing the Induction Hardening Process of C45 Spur-Gear. *Metals* **2023**, *13*, 997. [CrossRef]

32. Asadzadeh, M.Z.; Roppert, K.; Raninger, P. Material Data Identification in an Induction Hardening Test Rig with Physics-Informed Neural Networks. *Materials* **2023**, *16*, 5013. [CrossRef] [PubMed]

33. Denk, F.; Haehre, K.; Simon, C.; Eizaguirre, S.; Heidinger, M.; Kling, R.; Heering, W. 25 kW High Power Resonant Inverter Operating at 2.5 MHz based on SiC SMD phase-leg modules. In Proceedings of the PCIM Europe 2018: International Exhibition and Conference for Power Electronics, Intelligent Motion, Renewable Energy and Energy Management, Nuremberg, Germany, 5–7 June 2018.

34. Haema, J.; Phudungthin, R. Full bridge resonant inverter for blade induction heating application. *Energy Procedia* **2019**, *156*, 391–395. [CrossRef]

35. Hammouma, C.; Zeroug, H. Enhanced frequency adaptation approaches for series resonant inverter control under workpiece permeability effect for induction hardening applications. *Eng. Sci. Technol. Int. J.* **2022**, *27*, 101006. [CrossRef]

36. Kierepka, K.; Legutko, P.; Zimoch, P.; Kasprzak, M. Dual-frequency induction heating for gear hardening: Converter, resonant circuit, and FEM modelling. *IET Power Electron.* **2018**, *11*, 2396–2402. [CrossRef]

37. Kilic, V.T.; Unal, E.; Demir, H.V. High-efficiency flow-through induction heating. *IET Power Electron.* **2020**, *13*, 2119–2126. [CrossRef]

38. ALLDATASHEET. Available online: https://www.alldatasheet.com/datasheet-pdf/pdf/27318/TI/SG3524.html (accessed on 11 July 2023).

39. ALLDATASHEET. Available online: https://www.alldatasheet.com/datasheet-pdf/pdf/609004/IRF/IR2213.html (accessed on 11 July 2023).

40. Kokuhennadige, Y.; Billah, M.M.; Hietanen, J.-M.; Lind, J. *Induction Heater for Melting Aluminum*; School of Electrical Engineering, Automation and Electrical Engineering (AEE) Master's Programme; Aalto University: Helsinki, Finland, 2019.

41. Radetić, R. *Small Induction Heating Devices—Theory and Practice*; Infoelektronika: Niš, Serbia, 2019.